

Ion temperature effects on plasma flow in the magnetic mirror configuration

A. Sabo,¹ A. I. Smolyakov,¹ P. Yushmanov,² and S. Putvinski²

¹⁾ *University of Saskatchewan, Saskatchewan, Saskatoon SK S7N 5E2, Canada*

²⁾ *TAE Technologies, 19631 Pauling, Foothill Ranch, CA, 92610, United States*

Effects of finite ion temperature on plasma flow in the converging-diverging magnetic field, the magnetic mirror, or equivalently, magnetic nozzle configuration, are studied using a quasineutral paraxial two-fluid MHD model with isothermal electrons and warm magnetized ions. The ion acceleration was studied with an emphasis on the role of the singularity at the sonic point transition. It is shown that the regularity of the sonic point defines a global solution describing plasma acceleration from subsonic to supersonic velocity. Stationary accelerating solutions were obtained and compared with the time dependent dynamics, confirming that the solutions of the time-dependent equations converge to the stationary solutions and therefore are stable. The effects of the ion pressure anisotropy were analyzed using Chow-Golberger-Law model and its generalization. It is shown that the mirror force (manifested by the perpendicular ion pressure) enhances plasma acceleration. The role of ionization and charge exchange on plasma flow acceleration have been investigated.

Keywords: Plasma acceleration, magnetic nozzle, anisotropic pressure, CGL, mirror machine

I. INTRODUCTION

The plasma flow in the magnetic mirror configuration (magnetic nozzle) plays an important role in a number of devices, such as magnetic mirrors used in fusion research and devices for electric propulsion in space. In plasma propulsion, magnetic nozzle configuration is employed to convert the plasma thermal energy into the ion kinetic energy, thus generating thrust^{1,2}. In open mirror fusion devices, the expanding magnetic field of the divertor (expander region) is used to spread the energy over the larger area to reduce the wall heat loads³. Plasma flow in the edge region of the divertor tokamak also experiences acceleration to supersonic velocities due to the combined effects of plasma pressure and inhomogeneous magnetic field⁴⁻⁶. Various aspects of plasma flow and acceleration in the magnetic mirror configurations have been studied. General framework of plasma flow and acceleration in the MHD approximation was formulated in Ref. 7, and subsequently used to study plasma detachment⁸, acceleration mechanisms and propulsion efficiency^{9,10}. The role of the magnetic nozzle in the conversion of plasma thermal energy to supersonic flow was demonstrated experimentally^{11,12}. The MHD models were used to study the supersonic acceleration in scrape-off-layer (SOL) of tokamak edge in Refs. 13–15. Ion pressure anisotropy and related mirror force effects on the plasma flow in the SOL were considered and the predictions of the isotropic and anisotropic pressure models were compared for specific conditions of the advanced divertors in fusion systems in Refs. 14 and 15. The emphasis of this paper is on the role of the sonic point transition in the formation of the accelerating potential in plasma with anisotropic ion pressure and including the atomic processes such as ionization and charge exchange.

It is well known that in the quasineutral approximation the ion inertia and finite temperature result in the appearance of the sonic point singularity at the point where the local ion velocity is equal to the ion sound speed c_s . It has recently been emphasized¹⁶ that the conditions at the sonic point in the nozzle region where the magnetic field has the maximum are critical for the existence of the smooth accelerating solution such that the resulting plasma flow is uniquely defined in the whole converging-diverging region, i.e. in the whole range from sub-sonic, $V < c_s$, to super-sonic, $V > c_s$, velocities. Such smooth accelerating solution is formed by the ambipolar potential supported by the electron pressure gradient. Here we study how the addition of the ion pressure, its anisotropy, in particular, the effects of the

mirror force, and some dissipative processes modify the conditions for the formation of a smooth accelerating potential. These results are of interest for fusion devices application^{3,15} as well as for the propulsion devices where a large ion temperature is expected².

The basic model equations are presented in Section II. The Section III discusses general features of the sonic point singularity and ion acceleration with finite ion pressure. Plasma acceleration for cold ions is reviewed in Section IV. The Section V presents the results of the solution of the stationary and dynamic (time-dependent) equations for the base case with anisotropic pressure. The Section VI analyzes modifications due to the ionization and charge-exchange collisions. The summary and discussions are presented in Section VII.

II. BASIC MODEL

In our model electrons are considered in the massless isothermal $T_e = \text{const}$ approximation,

$$0 = en \frac{\partial \phi}{\partial z} - T_e \frac{\partial n}{\partial z}. \quad (1)$$

The ions are described by the two-pressure Chow-Goldberger-Law (CGL) model¹⁷ in the form

$$\frac{d}{dt} \left(\frac{p_{\parallel} B^2}{n^3} \right) = S_{\parallel}, \quad (2)$$

$$\frac{d}{dt} \left(\frac{p_{\perp}}{nB} \right) = S_{\perp}, \quad (3)$$

where p_{\perp} and p_{\parallel} are the perpendicular and parallel ion pressure, respectively. The standard CGL model is generalized here to include the sink terms S_{\perp} , S_{\parallel} due to dissipation related to ionization and charge-exchange. We consider a problem in the paraxial approximation so that the total fluid time derivative for ions is $d/dt = \partial/\partial t + V_{\parallel} \nabla_{\parallel}$, where $V_{\parallel} = \mathbf{V} \cdot \mathbf{B}/B$ is the ion parallel velocity, $\nabla_{\parallel} = \mathbf{b} \cdot \nabla = \mathbf{B}/B \cdot \nabla$, and $\mathbf{b} = \mathbf{B}/B$ represents a unit vector in the direction of the magnetic field.

In the paraxial approximation, the ion continuity and momentum equations take the form

$$\frac{\partial n}{\partial t} + B \frac{\partial}{\partial z} \frac{n V_{\parallel}}{B} = S_n, \quad (4)$$

$$m_i n \left(\frac{\partial V_{\parallel}}{\partial t} + V_{\parallel} \frac{\partial V_{\parallel}}{\partial z} \right) = -en \frac{\partial \phi}{\partial z} - \nabla p - \mathbf{b} \cdot \nabla \boldsymbol{\pi} + S_V. \quad (5)$$

The effects of anisotropic pressure are included in the momentum equation with anisotropic pressure tensor $\boldsymbol{\pi} = (p_{\parallel} - p_{\perp})(\mathbf{b}\mathbf{b} - \mathbf{I}/3)$, $p = (2p_{\perp} + p_{\parallel})/3$,. and where S_n, S_V describe the ionization source/sink effects.

In the context of the plasma flow and acceleration along the open magnetic field lines, the anisotropic MHD equations were considered in Refs. 18 and 19. Similar equations also follow from the drift-kinetic²⁰ or gyro-fluid equations^{21,22}. In simulations of plasma flow in the SOL tokamak regions the fluid models with additional source/sink terms in the density, momentum, and energy equations as well as model approximations for the heat fluxes and relaxation terms were used¹⁵. In this paper, our emphasis is on the ion pressure effects, so we use the standard adiabatic CGL equations¹⁷ modified with the model sink terms S_{\parallel} and S_{\perp} to model the effects of ionization and charge-exchange on the ion pressure evolution, cf. Eqs. (2) and (3).

In general, ionization contributes to the density, ion momentum and pressure evolution, while the charge exchange affects the ion momentum and pressure evolution. In the context of fusion and electric propulsion, the ionization by electron impact is most relevant. The ionization coefficients depend on the neutral species, neutral density, electron temperature and electron density, while charge-exchange coefficients depend on the ions/neutral density and their energy. Thus the ionization and charge-exchange effects may have complex profile dependencies depending on the particular situation and plasma parameters. In this study we are interested in the main parametric trends due to the ionization and charge exchange. Thus, we use a simplified model^{23,24} where the effects of ionization and charge exchange are represented by two constant coefficients ν_1 and ν_2 . The ν_1 coefficient corresponds to the ionization, while the ν_2 coefficient in the ion momentum equation describes the total effects of ionization and charge-exchange. In this study we neglect the heat flux effects in the energy (pressure evolution) as well as any possible ionization heating terms²⁵ and only the pressure "decay" terms are included with the same coefficient ν_2 for p_{\parallel} and p_{\perp} . In the expanded form, the full systems of equations including the ionization and charge-exchange effects is then written in the form similarly to Ref. 3:

$$\frac{\partial n}{\partial t} = nV_{\parallel} \frac{\partial \ln B}{\partial z} - V_{\parallel} \frac{\partial n}{\partial z} - n \frac{\partial V_{\parallel}}{\partial z} + \nu_1 n, \quad (6)$$

$$m_i n \left(\frac{\partial V_{\parallel}}{\partial t} + V_{\parallel} \frac{\partial V_{\parallel}}{\partial z} \right) = -en \frac{\partial \phi}{\partial z} - \frac{\partial p_{\parallel}}{\partial z} + (p_{\parallel} - p_{\perp}) \times \frac{\partial \ln B}{\partial z} - \nu_2 m_i n V_{\parallel}, \quad (7)$$

$$\frac{\partial p_{\parallel}}{\partial t} = p_{\parallel} V_{\parallel} \frac{\partial \ln B}{\partial z} - V_{\parallel} \frac{\partial p_{\parallel}}{\partial z} - 3p_{\parallel} \frac{\partial V_{\parallel}}{\partial z} - \nu_2 p_{\parallel}, \quad (8)$$

$$\frac{\partial p_{\perp}}{\partial t} = 2p_{\perp} V_{\parallel} \frac{\partial \ln B}{\partial z} - V_{\parallel} \frac{\partial p_{\perp}}{\partial z} - p_{\perp} \frac{\partial V_{\parallel}}{\partial z} - \nu_2 p_{\perp}. \quad (9)$$

We have to note that here we do not consider the plasma source region but focus on *plasma acceleration* in the magnetic mirror region, $0 < z < L$. Thus, effects of ionization and charge exchange, represented by the ν_1 and ν_2 in coefficients in the continuity, momentum, and pressure equations, are the model approximations for the ionization and charge-exchange effects in the magnetic mirror, while the plasma source is assumed for $z < 0$.

Before we proceed with the general case, we consider general conditions for the existence of accelerating solution and describe plasma acceleration for cold and warm ions in the absence of ionization and charge-exchange effects.

III. THE SONIC POINT SINGULARITY AND PLASMA ACCELERATION

In this section we consider a general condition for the existence of the global stationary accelerating solution in the absence of ionization and charge-exchange but taking into account anisotropic ion pressure. Setting $\nu_1 = \nu_2 = 0$, for the stationary case one can obtain from (1 - 9) the following equation for the ion velocity

$$\left(M^2 - 1 - \frac{3p_{\parallel}}{nT_e} \right) \frac{\partial M}{\partial z} = - \left(1 + \frac{p_{\perp}}{nT_e} \right) M \frac{\partial \ln B}{\partial z}. \quad (10)$$

In equation (10), $M = V_{\parallel}/c_s$ is the plasma velocity V_{\parallel} normalized to the speed of sound with respect to the electron velocity $c_s = \sqrt{(T_e/m_i)}$. Such normalization is convenient because T_e is constant and uniform. It is important to note that for warm anisotropic ions, the actual sound velocity includes the parallel ion temperature, $v_{cs} = \sqrt{(T_e + 3T_{i\parallel})/m_i}$. This is reflected in the modification of the sonic point singularity in equation (10), which occurs at a point where the ion velocity is equal to the local ion sound velocity, $M = M_{cr} = \sqrt{1 + 3p_{\parallel}/nT_e}$. We note that the expression $v_{cs} = \sqrt{(T_e + T_{i\parallel})/m_i}$ used for sound speed in some papers^{15,26} is incorrect and thus misrepresents the location of the transition point.

Equation (10) describes the ion acceleration with finite anisotropic pressure and is a generalization of the cold ions case¹⁶. This equation has to be solved simultaneously with equations (8) and (9) for p_{\perp} and p_{\parallel} . The acceleration is provided by the electron pressure and is enhanced by the ion perpendicular pressure. This effect, manifested by the p_{\perp} term on the right hand side of (10), is the results of the mirror force acting on ions with a finite perpendicular energy.

Generally supersonic acceleration in the magnetic mirror configuration is similar to the Laval nozzle acceleration. For the low velocity $M < M_{cr}$, the acceleration occurs due to the effective area cross-section decrease due to the magnetic field rise, $\partial \ln B / \partial z > 0$. After the critical point $M > M_{cr}$, in the region of decreasing magnetic field with $\partial \ln B / \partial z < 0$ the acceleration occurs in the supersonic regime supported by the electric field generated by the electron and ion pressure. Note that in both, subsonic and supersonic, regions the perpendicular pressure enhances the acceleration.

Equation (10) exhibits the singularity at $M = M_{cr}$, the point where the ion flow resonates with the ion sound mode. A global smooth accelerating solution can be obtained by regularizing the sonic point at the point $z = z_m$ where $\partial \ln B / \partial z = 0$, which therefore requires the condition

$$\left| M^2 - 1 - \frac{3p_{\parallel}}{nT_e} \right|_{z=z_m} = 0. \quad (11)$$

Expanding the left and right sides of (10) near the singular point and using equation (11) one obtains the expression for the $\partial M / \partial z$ derivative near $z = z_m$:

$$\begin{aligned} \left(\frac{\partial M}{\partial z} \right)^2 &= - \frac{(1 + p_{\perp}/nT_e)(1 + 3p_{\parallel}/nT_e)}{2(1 + 6p_{\parallel}/nT_e)} \frac{\partial^2 \ln B}{\partial z^2} \Bigg|_{z=z_m} \\ &= - \frac{(1 + T_{\perp}/T_e)(1 + 3T_{\parallel}/T_e)}{2(1 + 6T_{\parallel}/T_e)} \frac{\partial^2 \ln B}{\partial z^2} \Bigg|_{z=z_m}. \end{aligned} \quad (12)$$

This expression illustrates that the condition $\partial^2 \ln B / \partial z^2 < 0$, i.e. maximum of the magnetic field, for $z = z_m$, is required for the existence of a smooth (regular) solution. Note that the condition (12), for $\partial^2 \ln B / \partial z^2 < 0$, also allows the decelerating solution with $\partial M / \partial z < 0$. However, in the absence of plasma sources and sinks, no real solutions may exist in the case of the magnetic field minimum, for $\partial^2 \ln B / \partial z^2 > 0$.

IV. THE ACCELERATING POTENTIAL FOR THE CASE OF COLD IONS

In this section we overview the case of cold ions providing a simple illustration of the global properties of the accelerating potential formed by the converging-diverging magnetic field configuration. For $p_{\perp} = p_{\parallel} = 0$, Eq.(10) can be integrated^{27,28} resulting in the implicit equation for the ion velocity in the form

$$\frac{M^2}{2} - \frac{1}{2} = - \ln \left(\frac{B(z)}{M(z) B_m} \right). \quad (13)$$

In this case of cold ions, the ion sound velocity is c_s and the singularity occurs for $M = 1$. Here $B_m = B(z)$ at $z = z_m$ and the integration constant was chosen so the solution is regular at $z = z_m$ where $M = 1$. From Eq. (13) one can find that the velocity derivative $\partial M / \partial z$ is

$$\left(\frac{\partial M}{\partial z} \right)^2 = - \left. \frac{1}{2} \frac{\partial^2 \ln B}{\partial z^2} \right|_{z=z_m}. \quad (14)$$

Generally, acceleration of the magnetized plasma in the magnetic nozzle is analogous to the gas flow in Laval nozzle. It is also similar to the problem of the solar wind acceleration when the effective nozzle is created by the spherical expansion and the gravity force²⁹. The exact solution for equation (13) can be written¹⁶ in terms of the Lambert function which appears in various fields including numerous plasma physics applications^{30–32}. The solution for spherically expanding solar wind can also be written with the Lambert function³³.

Here, for illustration, we consider the magnetic field mirror with Gaussian profile, $B(z) = (B_m - B_0) \exp(- (z - z_0)^2 / (\delta^2 L^2)) + B_0$, giving a mirror ratio $R = B_m / B(z) = 4$ at both ends, $z = 0$ and $z = L$. Several cases with different widths were considered by changing δ , as shown in Fig. 1a. Also, different values of the mirror ratio were considered by changing the value of both δ and B_0 .

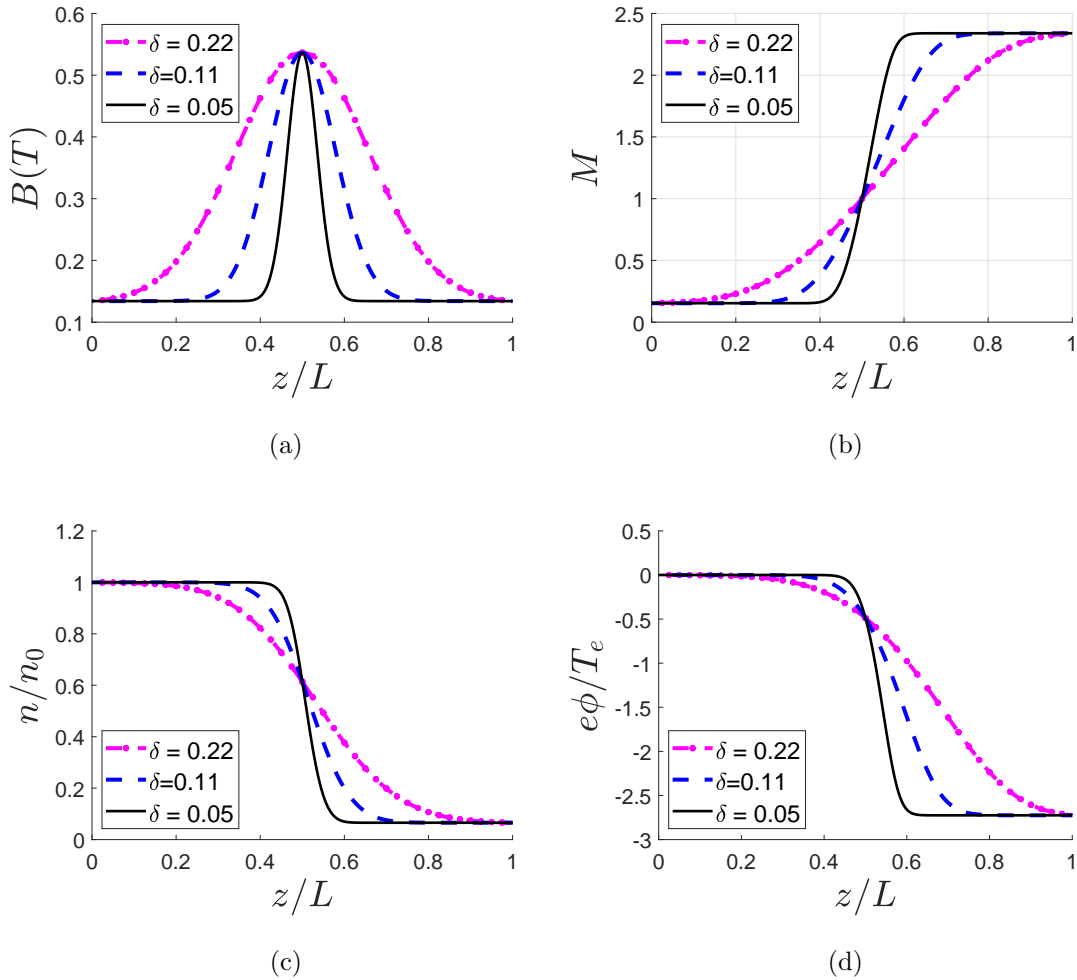


FIG. 1: Acceleration of cold ions in the magnetic field with mirror ratio $R = B_m/B(0) = 4$, $B(0) = B(L)$ The axial profiles for a) magnetic field, b) Mach number, c) plasma density and d) electrostatic potential, for different values of the magnetic mirror width δ .

Equation (13) shows that the local value of the plasma velocity is defined by the local value of the magnetic field. It is important to note that this solution has a global character defined by the regularization condition at the sonic point, $V_{\parallel} = c_s$. For cold plasma, the sonic point is at $\partial \ln B / \partial z = 0$, and the condition for the regular (smooth) solution defines the velocity derivative at this point, therefore fixing the velocity profile globally. Note that for isothermal electrons the absolute value of plasma density n scales out. In what follows, we show the plasma density normalized to the value n_0 at $z = 0$:

$$\frac{n(z)V_{\parallel}(z)}{B(z)} = \frac{n_0V_{\parallel 0}}{B(0)}. \quad (15)$$

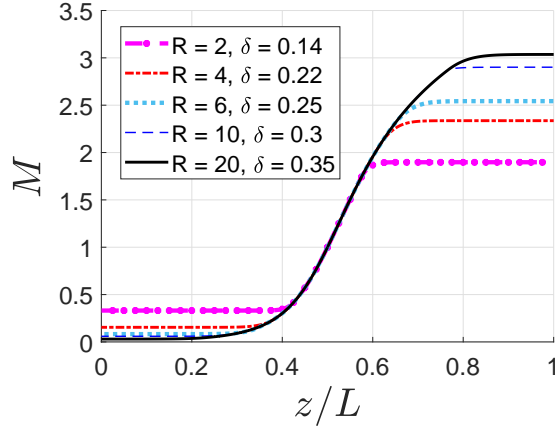


FIG. 2: Plasma velocity profiles for different values of the mirror ratio.

One can see from equation (13) that the sub-sonic acceleration, $M(z) < 1$, is mostly due to the effective area decrease, while equations in the super-sonic regime, $M(z) > 1$, the acceleration is driven by the electric field due to the electron pressure. The velocity, density, and potential profiles for different values of δ and the same $R = 4$ mirror ratio are shown in the figures 1b, 1c, and 1d. Increase of the mirror ratio leads to the decrease of the initial velocity $M_0 \equiv M(0) < 1$, and increase of the exit velocity at $z = L$, $M_L \equiv M(L) > 1$. The plasma velocity at the nozzle exit only depends on the mirror ratio R (regardless of the details of the magnetic field profile), and has weak logarithmic divergence for $R \gg 1$, as is shown in Fig. 2.

V. EFFECT OF THE ANISOTROPIC ION TEMPERATURE ON PLASMA FLOW

In this Section, we present the global regular solutions for plasma flow with finite (and anisotropic) ion pressure for the magnetic field profile similar to the C-2U device^{3,34} shown in Fig. 3. The global solutions are considered in the region $0 < z < L$. The mirror ratios were $B_m/B_0 = 8.0$ and $B_m/B_r = 20.0$ at the left, $z = 0$, and the right, $z = L$, ends of the nozzle, respectively. The magnetic field setup is described in more detail in the Appendix. The left side of the simulation region represents the transition to the plasma source at $z < 0$. It is important to note that plasma velocity is fixed globally by the condition at the singular point, so that it cannot be taken arbitrary at $z = 0$; the value at the exit point, $z = L$ is

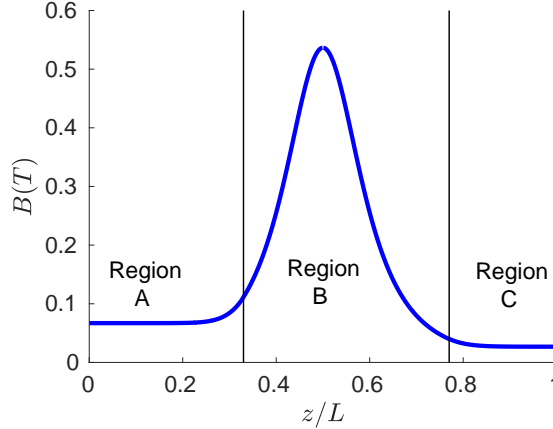


FIG. 3: Magnetic field of the mirror configuration as in Ref.3 and 34

uniquely fixed as well. We will discuss this constraint and its consequences further below.

The numerical solution of stationary equations (10) and (1 - 9) are obtained by the integration from the the proximity of the sonic point, $z_m/L = 0.5$, in both $z < z_m$ and $z > z_m$ directions. The initial conditions for the parameters M , n , p_{\parallel} , and p_{\perp} are obtained from the Taylor series expansion near $z = z_m$. Across the entire nozzle electrons were assumed to be isothermal with $T_e = 200$ eV. At the left end of the nozzle it was assumed that $T_{i\parallel 0} = T_{i\perp 0} = 200$ eV with the density $n_0 = 1.0 \times 10^{19} m^{-3}$, however all results can be represented in dimensionless units by being normalized to their respective values at $z = 0$. The shooting method was used to achieve the final solution with isotropic ion pressure, $T_{i\parallel 0} = T_{i\perp 0} = 200$ eV at the left end of the nozzle, which corresponds to the beginning of Region A in Fig. 3.

Similarly to the case of cold ions, plasma acceleration occurs in the regions with the finite gradient of the magnetic field. The perpendicular ion pressure enhances the ion acceleration according to equation (12). The parallel ion pressure shifts the sonic point which is now defined by Eq. (10). However, the parallel pressure decreases fast with distance, so the effects of the finite parallel pressure on the location of the singular point is weak for our parameters.

An interesting observation that can be seen from Fig. 4b is that for a finite ion temperature there is a region where the density is increasing with distance, contrary to the case of cold ions, where the density is always monotonically decreasing in regions of non constant

magnetic field. A similar behavior is observed for the potential, with the small increase with distance being displayed in Fig. 4f.

The perpendicular plasma pressure follows the increase of the magnetic field B related to the conservation of the adiabatic invariant as $T_{i\perp}(z)/B(z) = \text{const}$. The dependence of $T_{i\perp}, T_{i\parallel}$ on $B(z)$ are shown in Fig. 4e. The decrease of $T_{i\parallel}$ in the outer region is related to strong plasma density dependence $\sim n^3$ in the CGL equation of state for p_{\parallel} and density decrease due to plasma acceleration.

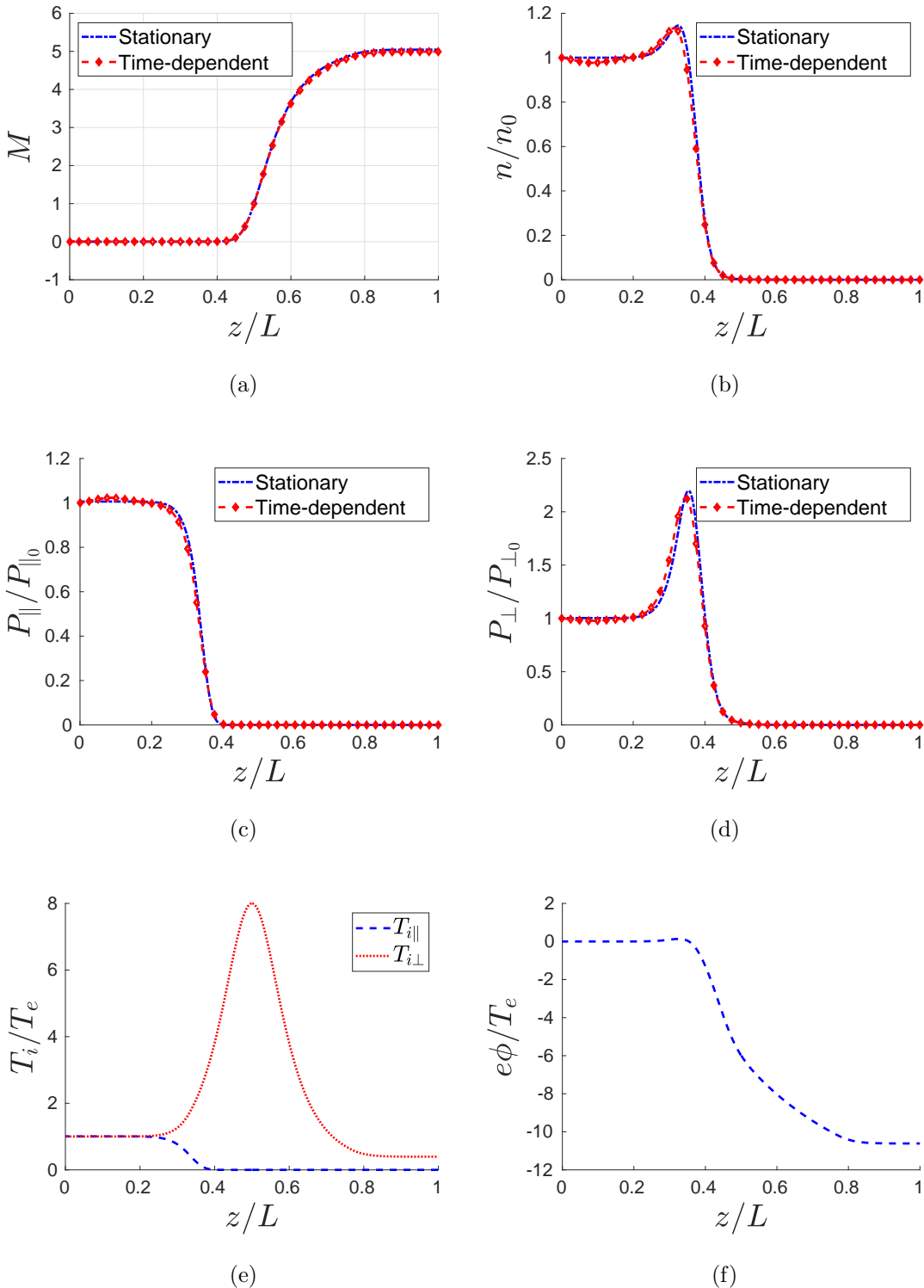


FIG. 4: Stationary solutions profiles for the case of $T_{i\parallel 0} = T_{i\perp 0} = 200$ eV: a) Mach number, b) plasma density, c) parallel pressure, d) perpendicular pressure, e) ion temperatures and f) electrostatic potential. Both solutions of stationary equations (obtained by shooting methods) and time-dependent initial value problem are shown in (a), (b), (c), and (d).

$T_{i\parallel 0}(eV)$	$T_{i\perp 0}(eV)$	M_0	M_L
200	400	2.85×10^{-7}	6.41
200	200	3.16×10^{-4}	5.04
200	100	0.01	4.18
200	50	0.06	3.66

TABLE I: Entrance, $z = 0$, and exit, $z = L$, plasma flow Mach number for different ion temperature at $z = 0$.

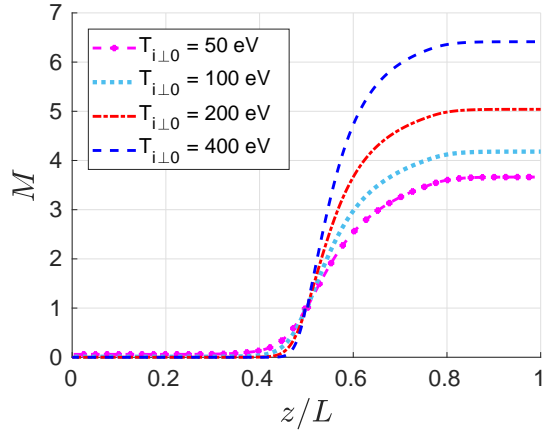


FIG. 5: Mach number M profiles for $T_{i\parallel 0} = 200$ eV and different $T_{i\perp 0}$ values

The perpendicular ion temperatures $T_{i\perp 0} = 200$ eV were changed to study the effect of perpendicular temperature at nozzle entrance $z = 0$. Three additional cases were studies with $T_{i\perp} = 400$ eV, $T_{i\perp} = 100$ eV, and $T_{i\perp} = 50$ eV, while $T_{i\parallel 0} = 200$ eV and $T_e = 200$ eV remained the same. For the initial anisotropic ion pressure state at $z = 0$, the finite perpendicular ion temperature increases the velocity of the accelerated ions as shown in Fig. 5 and displayed in Table I.

Steady-state solutions of stationary equations obtained by the shooting method were compared with the time-dependent solutions obtained as a solution of the initial value problem for equations (6 - 9), presented in the Appendix with additional details. We have verified that the solution of the time-dependent equations converge well to the stationary solution obtained by the shooting method, as shown in figures 4a, 4b, 4c and 4d. The character-

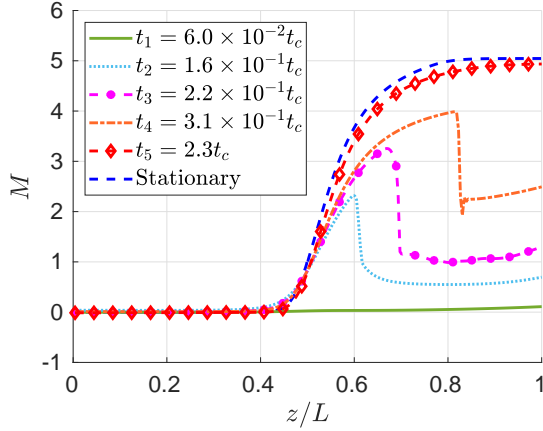


FIG. 6: Time evolution of the velocity profile obtained in the time dependent initial value problem.

istic time was $t_c = L/c_s = 4.0 \times 10^{-5} s$ and each time interval was given as a multiple of t_c . Each time step in the simulation was equivalent to $1.0 \times 10^{-5} t_c$. The evolution of the time-dependent problem toward the stationary solution is shown in Fig. 6 for the successive moments in time $t_1 < t_2 \dots < t_5$ with the lowest $t_1 = 6.0 \times 10^{-2} t_c$ and the stationary solution value being reached at $t = 2.4 t_c$. This exercise demonstrates that the stationary accelerating solutions are stable and therefore dynamically accessible in the initial value problem.

VI. IONIZATION AND CHARGE-EXCHANGE EFFECTS

In this section we consider the ion flow taking into account the ionization and charge-exchange effects. These effects are important in fusion applications due to presence of neutrals in the mirror region. Effects of neutrals were also considered in propulsion applications. Depending on the application, neutral density and therefore ionization and charge-exchange rates may vary in a rather wide range^{3,35}. To estimate possible effects at various conditions, here we use generic form of the sink terms S_{\parallel} and S_{\perp} with various values of ν_1 and ν_2 in normalized form $\nu'_2 = \nu_2 L/c_s$, $\nu'_1 = \nu_1 L/c_s$ from low to large values. These rates are assumed constant throughout the nozzle. The rest of plasma parameters are normalized to their respective values at the left end of the nozzle such that $n' = n/n_0$, $p'_{\parallel} = p_{\parallel}/p_{\parallel 0}$, $p'_{\perp} = p_{\perp}/p_{\perp 0}$, $T'_{i\parallel} = T_{i\parallel}/T_e$, $T'_{i\perp} = T_{i\perp}/T_e$, $z' = z/L$ and $t' = c_s t/L$. (For the sake of convenience all the primes on parameters will be dropped and it will be assumed that n , p_{\parallel} , p_{\perp} , $T_{i\parallel}$, $T_{i\perp}$, ν_1 ,

ν_2 , z and t represent normalized quantities). In dimensionless form the stationary equations describing ion dynamics have the form

$$\frac{\partial n}{\partial z} = n \left(\frac{\partial \ln B}{\partial z} - \frac{1}{M} \frac{\partial M}{\partial z} + \frac{\nu_1}{M} \right), \quad (16)$$

$$\frac{\partial p_{\parallel}}{\partial z} = p_{\parallel} \left(\frac{\partial \ln B}{\partial z} - \frac{3}{M} \frac{\partial M}{\partial z} - \frac{\nu_2}{M} \right), \quad (17)$$

$$\frac{\partial p_{\perp}}{\partial z} = p_{\perp} \left(2 \frac{\partial \ln B}{\partial z} - \frac{3}{M} \frac{\partial M}{\partial z} - \frac{\nu_2}{M} \right), \quad (18)$$

$$\begin{aligned} \left(M^2 - 1 - \frac{3p_{\parallel}}{n} \frac{T_{i\parallel 0}}{T_e} \right) \frac{\partial M}{\partial z} = & - \left(1 + \frac{p_{\perp}}{n} \frac{T_{i\perp 0}}{T_e} \right) M \frac{\partial \ln B}{\partial z} \\ & + \left(\frac{p_{\parallel}}{n} \frac{T_{i\parallel 0}}{T_e} - M^2 \right) \nu_2 - \nu_1, \end{aligned} \quad (19)$$

$$\phi = T_e \ln \left(\frac{n}{n_0} \right). \quad (20)$$

Additional terms in Eq. (19) due to the ionization and charge-exchange effects modify the regularization condition at the sonic point. The sonic point is still defined by the condition 11. However the location of the sonic point, where the right hand side of equation (19) is zero is shifted from $z = z_m$. Expanding near the point, where both sides of Eq. (19) equal zero, we obtain for $\partial M/\partial z$ the following equation

$$a \left(\frac{\partial M}{\partial z} \right)^2 + b \left(\frac{\partial M}{\partial z} \right) + c = 0, \quad (21)$$

where

$$a = 2 \left(1 + \frac{6T_{i\parallel m}}{T_e} \right), \quad (22)$$

$$\begin{aligned} b = & \frac{5T_{i\parallel m}}{T_e} \nu_2 + \frac{3T_{i\parallel m}}{T_e} \nu_1 + \left(1 + \frac{T_{i\perp m}}{T_e} \right) \left(1 + \frac{3T_{i\parallel m}}{T_e} \right)^{\frac{1}{2}} \\ & \times \frac{\partial \ln B}{\partial z} + 2 \left(1 + \frac{3T_{i\parallel m}}{T_e} \right) \nu_2, \end{aligned} \quad (23)$$

$$\begin{aligned} c = & \left(1 + \frac{T_{i\perp m}}{T_e} \right) \left(1 + \frac{3T_{i\parallel m}}{T_e} \right) \frac{\partial^2 \ln B}{\partial z^2} + \frac{T_{i\perp m}}{T_e} \\ & \times \left(1 + \frac{3T_{i\parallel m}}{T_e} \right) \left(\frac{\partial \ln B}{\partial z} \right)^2 - \frac{T_{i\perp m}}{T_e} \left(1 + \frac{3T_{i\parallel m}}{T_e} \right)^{\frac{1}{2}} \\ & \times \frac{\partial \ln B}{\partial z} (\nu_2 + \nu_1) + \frac{T_{i\parallel m}}{T_e} (\nu_2 + \nu_1) \nu_2. \end{aligned} \quad (24)$$

Here $T_{i\parallel m}$ and $T_{i\perp m}$ are the values of the parallel and perpendicular temperature at the sonic point, which no longer occurs at $z = z_m$ but is shifted to the right. The shift in the location of the sonic is directly affected by the value of p_{\parallel} that is in turn affected by the values of ν_1 and ν_2 . Thus, higher values of ν_1 and ν_2 will have a more profound effect on p_{\parallel} and will indirectly shift the sonic point further away from its initial position at $z = z_m$. Similar to Section V, we obtain stationary solutions for equations (16) - (20) using the shooting method as described in Section III and compare these solutions with the solution of the initial value problem given by equations (1) - (9). Again, it has been confirmed that time-dependent solutions converge well to the stationary solutions after some relaxation.

There are several features introduced by ionization and charge-exchange effects. One is a non-monotonous behavior of plasma density with the increase due to the ionization, which is especially noticeable in the region of flat magnetic field before any substantial acceleration occurs. This behavior is more pronounced for higher ionization values, as indicated in Fig. 8d. Related to the density behavior, the potential also shows a non-monotonous increase in the region to the left of the maximum of the magnetic field as shown in Fig. 7e.

Another effect introduced by the dissipative terms, is the modification of the perpendicular pressure profile so that it does not follow the increase in the magnetic field. The latter effect is much reduced by dissipation so the perpendicular pressure profile may become similar to the parallel pressure with almost monotonous decrease throughout the whole region, and both the parallel and perpendicular pressure having very similar profiles with $T_{i\parallel}$ and $T_{i\perp}$ as displayed in Figures 7c and 7d. With the above noted modifications, the resulting velocity has a significantly larger value at the left boundary, $M = 0.127$, compared with the case in the absence of charge-exchange and ionization, and a lower final acceleration value on the exit side of the nozzle. The reduction in the final value of acceleration is greater for higher charge-exchange values as shown in Fig. 7a but also in the case of ionization alone as shown in Fig. 8a. One has to note also that the presence of the dissipative terms due to the ionization and charge-exchange results in the shift of the position of the sonic point so it is no longer at the magnetic field maximum, as described by equation (21).

The effect of charge-exchange has been further studied for various values of ν_2 as shown in Table II and Figures 7a, 7b, 7c, 7d and 7e. In Table II, the values of M_0 and M_L represent the value of the Mach number at the $z/L = 0$ and $z/L = 1$ ends of the nozzle respectively. Further increase in ν_2 results in the non-monotonous behavior of the plasma velocity in the

outer region, namely Region C, where the magnetic field is almost flat, between $z/L = 0.8$ and $z/L = 1$, see Fig. 7a. The width of the region with the density increase on the left side of the mirror is also increasing with ν_2 as shown in Fig. 7b. The characteristic increase in the perpendicular pressure is well pronounced for $\nu_2 = \nu_1 = 0$, is smoothed out by finite values of ν_2 and eventually disappears for large values of ν_2 as shown in Fig. 7d. A similar behavior is observed for p_{\parallel} and p_{\perp} when only ionization is present, with the decrease being more pronounced for higher values of ν_1 as shown in Fig. 8b and Fig. 8c respectively. The reduction of the velocity at the exit side, corresponding to the end of Region C, is consistent with the lower overall drop in the electrostatic potential as shown in Fig. 7e and displayed in Table II.

ν_2	M_0	M_L	$(e\phi/T_e)_0$	$(e\phi/T_e)_L$
0	7.5×10^{-3}	3.32	0	-4.77
0.1	0.024	3.217	0	-4.6
0.35	0.054	2.981	0	-4.21
1.0	0.071	2.564	0	-3.83
1.44	0.077	2.348	0	-3.77
1.85	0.127	2.145	0	-3.71

TABLE II: Plasma Mach number and electrostatic potential for constant ionization $\nu_1 = 0.1$ and different values of charge-exchange ν_2

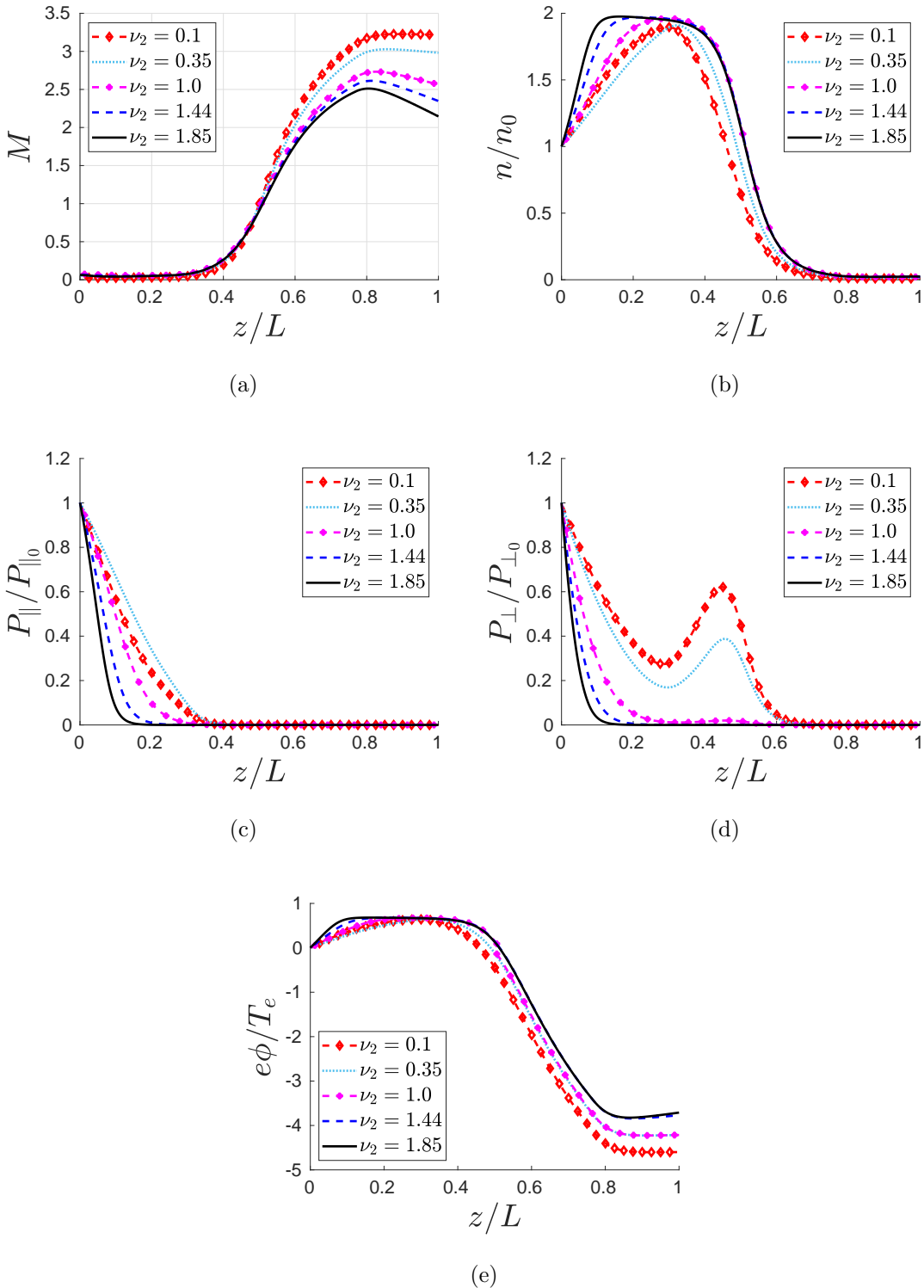


FIG. 7: Stationary solutions for the cases with constant ionization $\nu_1 = 0.1$ and different values of charge-exchange ν_2 for a) Mach number, b) plasma density, c) parallel pressure, d) perpendicular pressure and e) electrostatic potential.

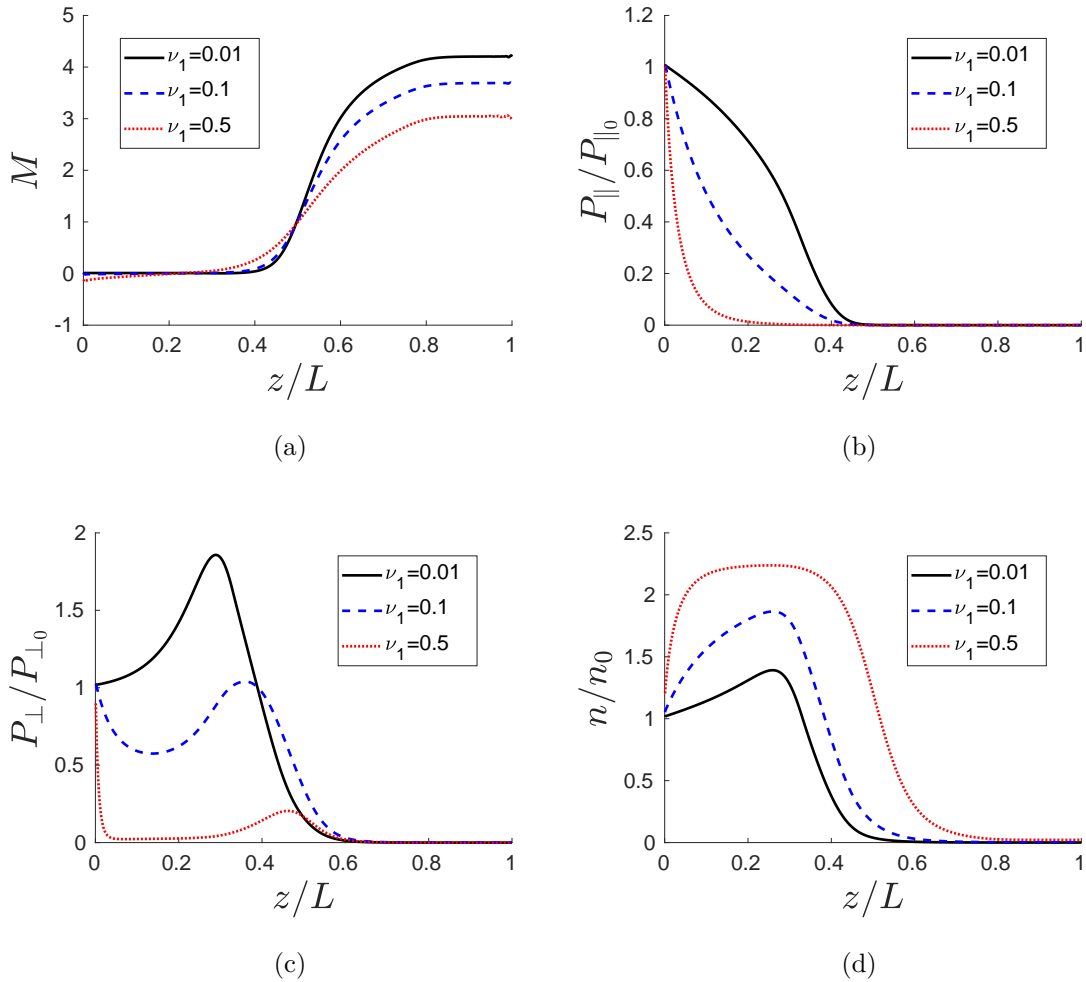


FIG. 8: Stationary solutions for the cases with constant charge-exchange $\nu_2 = 0$ and different values of ionization ν_1 : a) Mach number, b) parallel pressure, c) perpendicular pressure and d) plasma density.

VII. DISCUSSION AND CONCLUSIONS

The flow of plasma in a magnetic nozzle was studied in the paraxial approximation using fluid MHD model with fully magnetized ions and anisotropic pressure. Stiffness of the global acceleration profile, which is fully defined by the regularization condition at the sonic point, is one of the most important results of this manuscript. The unique accelerating solution starts with a finite (and fixed) value $V_{\parallel} < c_s$ at the entrance of the magnetic mirror. This solution continues through the sonic point $V_{\parallel} = c_s$ to the diverging region where the ion velocity

becomes supersonic. Plasma acceleration occurs as a result of an ambipolar electrostatic potential drop formed in the magnetic mirror, converting finite plasma pressure into the ion kinetic energy. We have shown that the finite perpendicular ion temperature increases the finite ion velocity in the exit region due to the effect of the mirror force. The finite (accelerated) value of the plasma velocity is defined by the electron and ion temperatures and the magnetic mirror aspect ratio. It is important to note that CGL theory is collisionless and the additional ion acceleration due to the perpendicular pressure is a result of the mirror force.

In most applications of interest, plasmas are collisionless, but coupling of plasma flow with neutrals was noted as an important factor for some fusion^{3,24} and plasma thruster applications^{36–38}. We have studied how the ionization and charge-exchange processes reform the accelerating potential impeding the plasma flow. We have shown that the ionization and charge-exchange shift the position of the sonic point from the maximum magnetic field, reduce plasma acceleration, and may result in non-monotonous behavior of plasma density and electrostatic potential.

We have obtained solutions of stationary equations with the shooting method. We have also performed simulations of time-dependent equations as an initial value problem therefore proving the stability of obtained stationary solutions.

Similarly to Refs. 39 and 40 our model is a paraxial approximation which considers the radial variations only in the main order. Though such one-dimensional models are often a good approximation for a full two-dimensional dynamics²⁸, two-dimensional effects are expected to be important⁹ for large diameter systems.

In general ion kinetic effects are important for low density collisionless plasma as in Refs. 3 and 34. One of the related limitations of the current study is the use of the standard collisionless two-pressure CGL model which neglects the ion heat fluxes. Further work is required to include heat fluxes either with extended two-pressure models and/or with full kinetic theory^{40,41}. It would be interesting to implement kinetic closures²¹ for the heat flux as proposed in Refs. 19. The kinetic ion model would also be required to describe the possible ion trapping and demagnetization effects for very low values of the magnetic field in the expander region. We have assumed fully magnetized ions and did not consider the detachment problem which may not be critical for fusion application, but would need to be analyzed for space propulsion applications⁴².

It is expected that electron cooling and trapped electrons in the region of the diverging magnetic field (expander) are important^{39,43,44}. Here, we have focused on ion dynamics and for simplicity assumed isothermal Boltzmann electrons. Effects of general polytropic equation of state for electrons with $\gamma \neq 1$ can be included similarly as in Ref. 16.

The obtained global solutions do not allow for arbitrary values of plasma velocity at the entrance point of the mirror region and also fully determine the plasma velocity at the mirror exit (fixed by the mirror ratio). The uniqueness of the accelerating solutions will therefore provide the constraints on the matter and energy outflow through the magnetic nozzle (mirror). These effects were not previously considered either in the context of open mirror or propulsion applications. These results raise interesting questions of how the plasma solutions in the source region can be matched to the mirror region. It is likely to occur via partial particle reflections (that have to be described kinetically) so that the total plasma flux is determined by the plasma density in the source region (effectively by the deposited power to produce plasma) due to define the plasma density in the source region.

ACKNOWLEDGMENTS

This work was supported in part by NSERC Canada and the U.S. Air Force Office of Scientific Research FA9550-15-1-0226 and FA9550-21-1-0031. Computational resources were provided by Compute Canada. The authors thank the investors of TAE Technologies and the entire TAE Team for their support.

DATA AVAILABILITY

Data generated in this study is available from the authors upon reasonable request.

REFERENCES

¹Igor D. Kaganovich, Andrei Smolyakov, Yevgeny Raitses, Eduardo Ahedo, Ioannis G. Mikellides, Benjamin Jorns, Francesco Taccogna, Renaud Gueroult, Sedina Tsikata, Anne Bourdon, Jean-Pierre Boeuf, Michael Keidar, Andrew Tasman Powis, Mario Merino, Mark Cappelli, Kentaro Hara, Johan A. Carlsson, Nathaniel J. Fisch, Pascal Chabert, Irina Schweigert, Trevor Lafleur, Konstantin Matyash, Alexander V. Khrabrov, Rod W. Boswell,

and Amnon Fruchtman. Physics of $E \times B$ discharges relevant to plasma propulsion and similar technologies. *Physics of Plasmas*, 27(12):120601, 2020.

²B. W. Longmier, E. A. Bering, M. D. Carter, L. D. Cassady, W. J. Chancery, F. R. C. Diaz, T. W. Glover, N. Hershkowitz, A. V. Ilin, G. E. McCaskill, C. S. Olsen, and J. P. Squire. Ambipolar ion acceleration in an expanding magnetic nozzle. *Plasma Sources Science & Technology*, 20(1):015007, 2011.

³M Onofri, P Yushmanov, S Detrick, D Barnes, K Hubbard, and T Tajima. Magnetohydrodynamic transport characterization of a field reversed configuration. *Physics of Plasmas*, 24(9):092518, 2017.

⁴H. Bufferand, G. Ciraolo, G. Dif-Pradalier, P. Ghendrih, P. Tamain, Y. Marandet, and E. Serre. Magnetic geometry and particle source drive of supersonic divertor regimes. *Plasma Physics and Controlled Fusion*, 56(12):122001, 2014.

⁵A. Kirk, W. Fundamenski, J. W. Ahn, and G. Counsell. Parallel sol transport in mast and jet: the impact of the mirror force. *Plasma Physics and Controlled Fusion*, 45(8):1445–1463, 2003.

⁶P. Ghendrih, K. Bodi, H. Bufferand, G. Chiavassa, G. Ciraolo, N. Fedorczak, L. Isoardi, A. Paredes, Y. Sarazin, E. Serre, F. Schwander, and P. Tamain. Transition to supersonic flows in the edge plasma. *Plasma Physics and Controlled Fusion*, 53(5):054019, 2011.

⁷AI Morozov and LS Solov'ev. Steady-state plasma flow in a magnetic field. pages 1–103. Springer, 1980.

⁸E. B. Hooper. Plasma detachment from a magnetic nozzle. *Journal of Propulsion and Power*, 9(5):757–763, 1993.

⁹E. Ahedo and M. Merino. Two-dimensional supersonic plasma acceleration in a magnetic nozzle. *Physics of Plasmas*, 17(7):073501, 2010.

¹⁰M. Merino and E. Ahedo. Fully magnetized plasma flow in a magnetic nozzle. *Physics of Plasmas*, 23(2):023506, 2016.

¹¹M. Inutake, K. Yoshino, S. Fujimura, H. Tobari, T. Yagai, Y. Hosokawa, R. Sato, K. Hattori, and A. Ando. Production of a high-mach-number plasma flow for an advanced plasma space thruster. *Plasma Science & Technology*, 6(6):2541–2545, 2004.

¹²M. Inutake, A. Ando, K. Hattori, H. Tobari, T. Makita, M. Shibata, Y. Kasashima, and T. Komagome. Generation of supersonic plasma flows using an applied-field mpd arcjet and icrf heating. *Plasma Physics and Controlled Fusion*, 49(5A):A121–A134, 2007.

¹³Rajiv Goswami, Jean-François Artaud, Frédéric Imbeaux, and Predhiman Kaw. Numerical study of transition to supersonic flows in the edge plasma. *Physics of Plasmas*, 21(7):072510, 2014.

¹⁴S. Togo, D. Reiser, P. Borner, M. Sakamoto, N. Ezumi, and Y. Nakashima. Benchmarking of b2 code with a one-dimensional plasma fluid model incorporating anisotropic ion pressures on simple mirror configurations. *Plasma and Fusion Research*, 13:3403022, 2018.

¹⁵S. Togo, T. Takizuka, D. Reiser, M. Sakamoto, N. Ezumi, Y. Ogawa, K. Nojiri, K. Ibano, Y. Li, and Y. Nakashima. Self-consistent simulation of supersonic plasma flows in advanced divertors. *Nuclear Fusion*, 59(7):076041, 2019.

¹⁶A. I. Smolyakov, A. Sabo, P. Yushmanov, and S. Putvinskii. On quasineutral plasma flow in the magnetic nozzle. *Physics of Plasmas*, 28(6):060701, 2021.

¹⁷GF Chew, ML Goldberger, and FE Low. The boltzmann equation and the one-fluid hydro-magnetic equations in the absence of particle collisions. *Proceedings of the Royal Society of London. Series A. Mathematical and Physical Sciences*, 236(1204):112–118, 1956.

¹⁸Emad Zawaideh, Farrokh Najmabadi, and Robert W Conn. Generalized fluid equations for parallel transport in collisional to weakly collisional plasmas. *The Physics of fluids*, 29(2):463–474, 1986.

¹⁹Zehua Guo, Xian-Zhu Tang, and Chris McDevitt. Parallel heat flux and flow acceleration in open field line plasmas with magnetic trapping. *Physics of Plasmas*, 21(10):102512, 2014.

²⁰A. I. Smolyakov and X. Garbet. Drift kinetic equation in the moving reference frame and reduced magnetohydrodynamic equations. *Physics of Plasmas*, 17(4):042105, 2010.

²¹P. B. Snyder, G. W. Hammett, and W. Dorland. Landau fluid models of collisionless magnetohydrodynamics. *Physics of Plasmas*, 4(11):3974–3985, 1997.

²²S. Robertson. A reduced set of gyrofluid equations for plasma flow in a diverging magnetic field. *Physics of Plasmas*, 23(4):043513, 2016.

²³P. Helander, S. I. Krasheninnikov, and P. J. Catto. Fluid equations for a partially-ionized plasma. *Physics of Plasmas*, 1(10):3174–3180, 1994.

²⁴Sheung-Wah Ng and A. B. Hassam. Neutral penetration in centrifugally confined plasmas. *Physics of Plasmas*, 14(10):102508, 2007.

²⁵B. Lehnert. Rotating plasmas. *Nuclear Fusion*, 11(5):485–533, 1971.

²⁶S. Togo, T. Takizuka, D. Reiser, M. Sakamoto, Y. Ogawa, N. Ezumi, K. Ibano, K. Nojiri, Y. Li, and Y. Nakashima. Characteristics of plasma flow profiles in a super-x-divertor-like configuration. *Nuclear Materials and Energy*, 19:149–154, 2019.

²⁷W. M. Manheimer and R. F. Fernsler. Plasma acceleration by area expansion. *Ieee Transactions on Plasma Science*, 29(1):75–84, 2001.

²⁸A. Fruchtman, K. Takahashi, C. Charles, and R. W. Boswell. A magnetic nozzle calculation of the force on a plasma. *Physics of Plasmas*, 19(3):033507, 2012.

²⁹E. N. Parker. Dynamics of the interplanetary gas and magnetic fields. *Astrophysical Journal*, 128(3):664–676, 1958.

³⁰Alexander E. Dubinov and Irina D. Dubinova. How can one solve exactly some problems in plasma theory. *Journal of Plasma Physics*, 71(05):715, 2005.

³¹J. L. Raimbault, L. Liard, J. M. Rax, P. Chabert, A. Fruchtman, and G. Makrinich. Steady-state isothermal bounded plasma with neutral dynamics. *Physics of Plasmas*, 14(1):013503, 2007.

³²Alexander E. Dubinov. Mathematical tricks for pseudopotentials in the theories of nonlinear waves in plasma. *Physics of Plasmas*, 2022.

³³Steven R. Cranmer. New views of the solar wind with the lambert w function. *American Journal of Physics*, 72(11):1397–1403, 2004.

³⁴M. W. Binderbauer, T. Tajima, M. Tuszewski, L. Schmitz, A. Smirnov, H. Gota, E. Garate, D. Barnes, B. H. Deng, E. Trask, X. Yang, S. Putvinski, R. Andow, N. Bolte, D. Q. Bui, F. Ceccherini, R. Clary, A. H. Cheung, K. D. Conroy, S. A. Detrick, J. D. Douglass, P. Feng, L. Galeotti, F. Giannanco, E. Granstedt, D. Gupta, S. Gupta, A. A. Ivanov, J. S. Kinley, K. Knapp, S. Korepanov, M. Hollins, R. Magee, R. Mendoza, Y. Mok, A. Necas, S. Primavera, M. Onofri, D. Osin, N. Rath, T. Roche, J. Romero, J. H. Schroeder, L. Sevier, A. Sibley, Y. Song, L. C. Steinhauer, M. C. Thompson, A. D. Van Drie, J. K. Walters, W. Waggoner, P. Yushmanov, K. Zhai, and T. A. E. Team. Recent breakthroughs on c-2u: Norman’s legacy. In T. Tajima and M. Binderbauer, editors, *Physics of Plasma-Driven Accelerators and Accelerator-Driven Fusion*, volume 1721 of *AIP Conference Proceedings*, page 030003, 2016.

³⁵M. Lieberman and A. Lichtenberg. *Principles of plasma discharges and materials processing*. (Wiley-Blackwell, 2005).

³⁶A. Fruchtman. Neutral gas depletion in low temperature plasma. *Journal of Physics D-Applied Physics*, 50(47):473002, 2017.

³⁷B. Wachs and B. Jorns. Background pressure effects on ion dynamics in a low-power magnetic nozzle thruster. *Plasma Sources Science & Technology*, 29(4):045002, 2020.

³⁸K. Takahashi, Y. Takao, and A. Ando. Neutral-depletion-induced axially asymmetric density in a helicon source and imparted thrust. *Applied Physics Letters*, 108(7):074103, 2016.

³⁹M. Merino, J. Maurino, and E. Ahedo. Kinetic electron model for plasma thruster plumes. *Plasma Sources Science and Technology*, 27(3):035013, 2018.

⁴⁰E. Ahedo, S. Correyero, J. Navarro-Cavallé, and M. Merino. Macroscopic and parametric study of a kinetic plasma expansion in a paraxial magnetic nozzle. *Plasma Sources Science and Technology*, 29(4):045017, 2020.

⁴¹Manuel Martinez-Sanchez and Eduardo Ahedo. Magnetic mirror effects on a collisionless plasma in a convergent geometry. *Physics of Plasmas*, 18(3):033509, 2011.

⁴²B. N. Breizman, M. R. Tushentsov, and A. V. Arefiev. Magnetic nozzle and plasma detachment model for a steady-state flow. *Physics of Plasmas*, 15(5):057103, 2008.

⁴³B. A. Wetherton, A. Le, J. Egedal, C. Forest, W. Daughton, A. Stanier, and S. Boldyrev. A drift kinetic model for the expander region of a magnetic mirror. *Physics of Plasmas*, 28(4):042510, 2021.

⁴⁴D. I. Skovorodin. Influence of trapped electrons on the plasma potential in the expander of an open trap. *Plasma Physics Reports*, 45(9):799–804, 2019.

Appendix A: Magnetic field profile

To study the effects of finite ion temperature we employed a mirror magnetic field. To simplify numerical calculations, the magnetic field was described by three different functions in regions A, B, and C: the region A, from $z' = z/L = 0$ to $z' = 0.33$, with $B_A(z') = 0.5e^{-84(z'-0.5)^2} + B_0$, $B_0 = 0.067$ (T); the region B from $z' = 0.33$ to $z' = 0.77$ with $B_B(z') = B_m (0.13)^3 / ((0.13)^2 + (z' - z_m)^2)^{\frac{3}{2}}$, where $B_m = 0.5365(T)$ is the magnetic field at the maximum at $z' = z_m$; the regions C from $z' = 0.77$ to $z' = 1$ with $B_C(z') = 0.55e^{-51(z'-0.5)} + B_r$, $B_r = 0.0268$ (T). The functions $B_A(z')$, $B_B(z')$, and $B_C(z')$ are chosen to have B and dB/dz continuous across the boundaries $A - B$ and $B - C$.

Appendix B: Time-dependent equations

The solutions of the stationary equations were verified with the initial value simulations of the time-dependent equations. In the absence of charge-exchange and ionization it has the following form:

$$\frac{\partial n}{\partial t} = nM \frac{\partial \ln B}{\partial z} - M \frac{\partial n}{\partial z} - n \frac{\partial M}{\partial z} + \alpha_1 \frac{\partial^2 n}{\partial z^2}, \quad (\text{B1})$$

$$\frac{\partial p_{\parallel}}{\partial t} = p_{\parallel}M \frac{\partial \ln B}{\partial z} - M \frac{\partial p_{\parallel}}{\partial z} - 3p_{\parallel} \frac{\partial M}{\partial z} + \alpha_2 \frac{\partial^2 p_{\parallel}}{\partial z^2}, \quad (\text{B2})$$

$$\frac{\partial p_{\perp}}{\partial t} = 2p_{\perp}M \frac{\partial \ln B}{\partial z} - M \frac{\partial p_{\perp}}{\partial z} - p_{\perp} \frac{\partial M}{\partial z} + \alpha_3 \frac{\partial^2 p_{\perp}}{\partial z^2}, \quad (\text{B3})$$

$$\begin{aligned} \frac{\partial M}{\partial t} = & -M \frac{\partial M}{\partial z} - \frac{1}{n} \frac{\partial n}{\partial z} - \frac{1}{n} \left(\frac{T_{i\parallel 0}}{T_e} \right) \frac{\partial p_{\parallel}}{\partial z} + \\ & \frac{1}{n} \left(\left(\frac{T_{i\parallel 0}}{T_e} \right) p_{\parallel} - \left(\frac{T_{i\perp 0}}{T_e} \right) p_{\perp} \right) \frac{\partial \ln B}{\partial z} + \alpha_4 \frac{\partial^2 M}{\partial z^2}. \end{aligned} \quad (\text{B4})$$

Here, with the exception of $T_{i\parallel 0}$, $T_{i\perp 0}$ and T_e , all quantities are expressed in dimensionless units. The diffusive coefficients α had the following values: $\alpha_1 = 5.0 \times 10^{-6}$, $\alpha_2 = 5.0 \times 10^{-6}$, $\alpha_3 = 5.0 \times 10^{-6}$ and $\alpha_4 = 1.0 \times 10^{-9}$.

Note that while the profiles of the density and pressure are fully determined by the global solution, the absolute values have free normalization parameters. Plasma parameters are normalized to their respective values at the left end of the nozzle such that $n' = n/n_0$, $p'_{\parallel} = p_{\parallel}/p_{\parallel 0}$, $p'_{\perp} = p_{\perp}/p_{\perp 0}$, $T'_{i\parallel} = T_{i\parallel}/T_e$, $T'_{i\perp} = T_{i\perp}/T_e$, $z' = z/L$ and $t' = c_s t/L$. (For the sake of convenience all the primes on parameters will be dropped and it will be assumed that n , p_{\parallel} , p_{\perp} , ϕ , $T_{i\parallel}$, $T_{i\perp}$, z and t represent normalized quantities).

The values for the diffusion coefficients α were small in comparison to the other terms in the equation and thus their addition did not affect the physics of the problem. For instance, for a value of $\alpha = 5.0 \times 10^{-6}$, $M = 3.179 \times 10^{-4}$ and $L = 4$ the condition $M/L = 7.95 \times 10^{-5} \gg \alpha/L^2 = 3.13 \times 10^{-7}$ holds.

When ionization and charge-exchange effects were included in the model, the time-dependent equations had the form

$$\begin{aligned}\frac{\partial n}{\partial t} = & nM \frac{\partial \ln B}{\partial z} - M \frac{\partial n}{\partial z} - n \frac{\partial M}{\partial z} + \nu_1 n \\ & + \beta_1 \frac{\partial^2 n}{\partial z^2},\end{aligned}\tag{B5}$$

$$\begin{aligned}\frac{\partial p_{\parallel}}{\partial t} = & p_{\parallel} M \frac{\partial \ln B}{\partial z} - M \frac{\partial p_{\parallel}}{\partial z} - 3p_{\parallel} \frac{\partial M}{\partial z} - \nu_2 p_{\parallel} \\ & + \beta_2 \frac{\partial^2 p_{\parallel}}{\partial z^2},\end{aligned}\tag{B6}$$

$$\begin{aligned}\frac{\partial p_{\perp}}{\partial t} = & 2p_{\perp} M \frac{\partial \ln B}{\partial z} - M \frac{\partial p_{\perp}}{\partial z} - p_{\perp} \frac{\partial M}{\partial z} - \nu_2 p_{\perp} \\ & + \beta_3 \frac{\partial^2 p_{\perp}}{\partial z^2},\end{aligned}\tag{B7}$$

$$\begin{aligned}\frac{\partial M}{\partial t} = & -M \frac{\partial M}{\partial z} - \frac{1}{n} \frac{\partial n}{\partial z} - \frac{1}{n} \left(\frac{T_{i\parallel 0}}{T_e} \right) \frac{\partial p_{\parallel}}{\partial z} + \\ & \frac{1}{n} \left(\left(\frac{T_{i\parallel 0}}{T_e} \right) p_{\parallel} - \left(\frac{T_{i\perp 0}}{T_e} \right) p_{\perp} \right) \frac{\partial \ln B}{\partial z} - \nu_2 M + \beta_4 \frac{\partial^2 M}{\partial z^2}.\end{aligned}\tag{B8}$$

The diffusion coefficients β were dimensionless and had the following values: $\beta_1 = 1.0 \times 10^{-3}$, $\beta_2 = 6.0 \times 10^{-3}$, $\beta_3 = 9.9 \times 10^{-4}$ and $\beta_4 = 1.0 \times 10^{-4}$.

Similar to the values of α , the values of β were small and did not affect the physics of the problem. For instance for $\beta = 1.0 \times 10^{-3}$, $M = 0.127$ and $L = 4$ the condition $M/L = 0.032 \gg \beta/L^2 = 6.25 \times 10^{-5}$ is true and the addition of the parameters β did not affect the physics of the problem.

The time-dependent equations describing the flow of plasma were solved in BOUT++. In the BOUT++ simulations, p_{\parallel} was displaying oscillatory behavior in region A of the nozzle. These oscillations were damped as t increased and the time-dependent value of p_{\parallel} approached the stationary solution value.